Journal of Hazardous Materials 311 (2016) 100–114

Contents lists available at ScienceDirect

Journal of Hazardous Materials

journal homepage: www.elsevier.com/locate/jhazmat

Improvements of the cyclone separator performance by down-comer tubes

Sakura Ganegama Bogodage*, A.Y.T. Leung

Department of Architectural and Civil Engineering, City University of Hong Kong, 83 Tat Chee Avenue, Kowloon, Hong Kong Special Administrative Region, China

HIGHLIGHTS

- Experiments were done on cyclone separators with/without bottom down-comer tubes.
- Cyclone performance parameters were evaluated for different solid loading rates.
- Discussed improvements of fine particle collection (PM 2.5) with down-comer tubes.
- Results were compared with established theories.

GRAPHICAL ABSTRACT

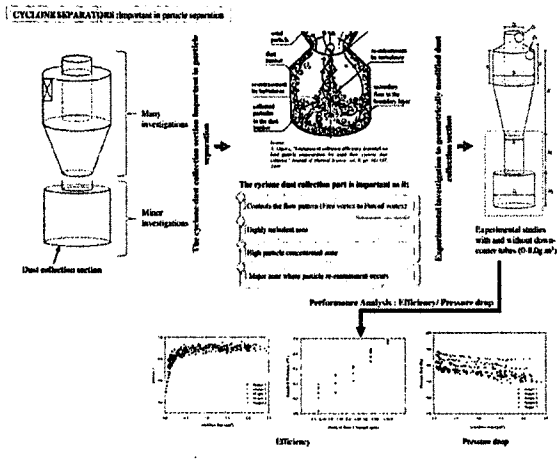

ARTICLE INFO

Article history:
Received 8 August 2015
Received in revised form 27 February 2016
Accepted 29 February 2016
Available online 4 March 2016

Keywords:
Cyclone separator
Down-comer tube
Solid loading rate
Pressure drop
Overall collection efficiency

ABSTRACT

Enhancement of fine particle (PM2.5) separation is important for cyclone separators to reduce any extra purification process required at the outlet. Therefore, the present experimental research was performed to explore the performance of cyclone separators modified with down-comer tubes at solid loading rates from 0 to 8.0 g/m^3 with a 10 m/s inlet velocity. The study proved the effectiveness of down-comer tubes in reducing the particle re-entrainment and increasing the finer separation with acceptable pressure drops, which was pronounced at low solid loading conditions. The experimental results were compared with theories of Smolik and Muschelknautz. Theories were acceptable for certain ranges, and theory breakdown was mainly due to the neglect of particle agglomeration, re-entrainment and the reduction of swirling energy, as well as the increase of wall friction due to presence of particles.

1. Introduction

Although cyclone separators are popular in today's particle-handling industry, the enhancement of fine particle collection is still a demanding topic. Filters or recirculation of processed air are usually combined with cyclone operation to increase the fine par-

* Corresponding author.
E-mail addresses: sganegama2-c@my.cityu.edu, sakurabogoda@gmail.com (S. Ganegama Bogodage).

http://dx.doi.org/10.1016/j.jhazmat.2016.02.072
0304-3894/

Nomenclature

A_R	Total wall area of cyclone contributes to frictional effect, m^2
a	Cyclone inlet height, m
B	Cyclone bottom/down-comer tube diameter, m
C	Solid loading rate (as a mass fraction)
C	Solid loading rate (concentration), g/m^3
$C_{(.)}$	Solid concentration, g/m^3
C_{0L}	Critical loading as a mass fraction
D	Cyclone body diameter, m
D_e	Vortex finder diameter, m
D_h	Hopper diameter, m
d	Particle diameter, μm
D_i, D_o	Inlet/outlet diameter of the tested cyclone, m
d_{fact}	Modification factor in Muschelknautz d_{50} equation
d_{50}	Cut size diameter, μm
f	Friction factor
f'	Frictional effect contributes with the effect of air and solid
H	Cyclone separator height, m
H_h	Hopper height, m
H_t	Down-comer tube height, m
h	Cyclone cylinder height, m
M_c	Mass of particles collected, g
M_{in}	Mass flow rate of incoming particles, g
MF_i	i^{th} mass fraction
P, p	Pressure, Pa
Q	Flow rate, m^3/s
R	Radius, m
S	Vortex finder height, m

Greek Letters

Δ	Difference in
η	Collection efficiency
θ	Tangential coordinate
μ	Dynamic viscosity of air, m^2/s
ρ	Density, kg/m^3

Subscripts

0	Start or reference
1, 2	Indicating spatial points or solids loadings
acc	Due to acceleration into the cyclone inlet
body	Cyclone body
CS	Cyclone control surface
e	Vortex finder
g	Gas
i	i^{th} fraction
in	Inlet
m	Geometric mean
p	Particle
str	Of a strand of solids
tot	Overall
w	Cyclone wall

ticle separation, which may increase the operational cost as well. Previous studies found that the major role of particle separation governs by the lower section of the cyclone separator due to effects of the natural vortex length of the flow, higher tangential velocities, particle re-entrainment and high particle concentrated zones [1–3]. However, further geometric modifications to this section are difficult (*i.e.*, the height of the cyclone cone and the diameter of the bottom opening) due to natural vortex length of the flow [1] (as quoted by Xiang et al. [4]).

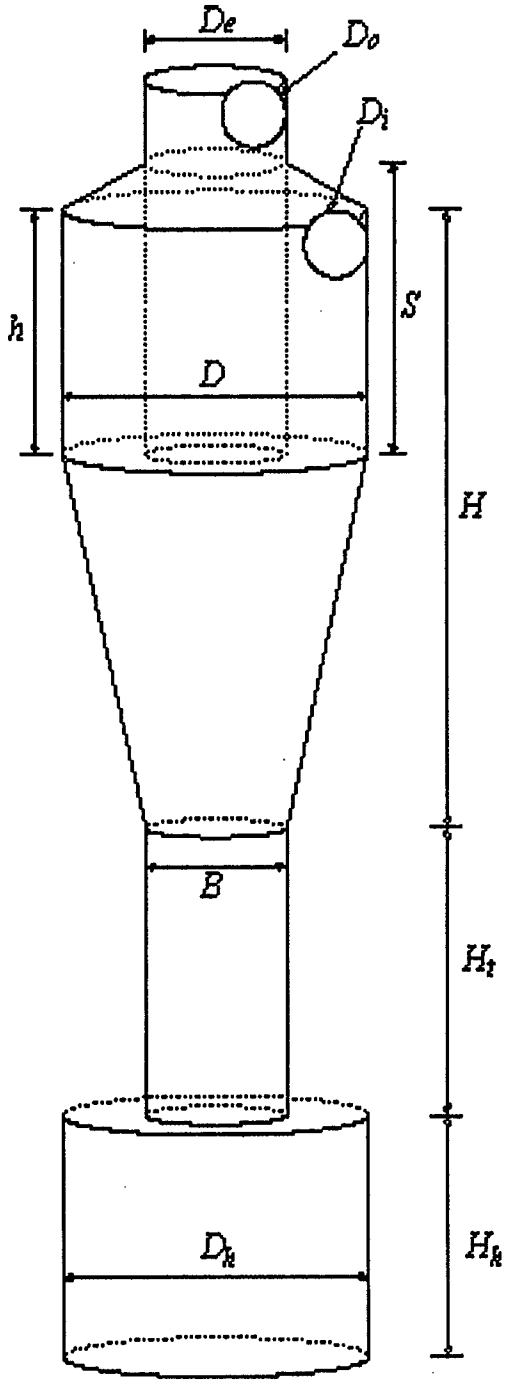

Fig. 1. Geometry of the cyclone separator.

The solid re-entrainment from the hopper is certain, as it is stifled at the cyclone bottom [5]. Mothes [2] investigated the movements of particles inside the cyclone separator and found higher particle concentrations near the cyclone bottom rather than at the cyclone inlet due to the particle concentrations that were 1) in the gas flow entering the dust collection hopper, and 2) re-entraining with the exit gas flow (as quoted by Obermair et al. [6]). This study indicated a requirement for control of particle re-entrainment from collection hoppers. However, in the literature, only a few studies investigated this section to minimize the solid re-entrainment from the dust collection hopper. For example, the studies modified the cyclone dust collection section by introducing apex cones [6–10], additional hoppers [6,9] and down-comer

Table 1
Geometric properties of the cyclone separator.

Geometric parameter	Dimension (mm)
Body diameter, D	330.200
Inlet/Outlet pipe diameters, D_i/D_o	69.120
Cyclone cylindrical body height, h	254.000
Cyclone total height, H	693.7375
Vortex finder height, S	303.2125
Vortex finder diameter, D_e	152.400
Cone tip diameter, B	152.400
Hopper height, H_h	254.000

Table 2
Dimensions of dust outlet geometries.

Dust outlet condition	Height of Down comer tube, H_t (mm)	Diameter of dust collection hopper, D_h (mm)
Hopper 1	0.0	152.4
Hopper 2	0.0	288.0
Hopper 3	127.0	288.0
Hopper 4	254.0	288.0
Hopper 5	381.0	288.0

tubes [5,6,9,11–14]. Among these, the cyclone separators modified with down-comer tubes showed a significant reduction in particle re-entrainment [6,9], even though the studies were performed at high solid loading rates. The efficient particle removal by down-comers in cyclone separators were analysed by Obermair et al. [6,15] using Phase Doppler Anemometry (PSD) investigations. The authors showed an increase in the tangential velocity inside the down-comer tubes by centrifuging particles onto the walls and back-mixing with the downward flow that restricts particle re-entrainment. None of these studies, however, have conducted a comprehensive analysis of the solid loading rate and the geometric effects of the cyclone dust collection section.

Investigation of cyclone separators with down-comers is significant due to the experimental uncertainties at high solid loading conditions, which are in turn due to the mass loading effect on particle separation [16] and dramatic reductions of the flow turbulence [17–19]. The present study therefore sought to explore the performance enhancement of fine particle separation based on down-comer height and particle loading rates. The cyclone performance parameters (collection efficiency and pressure drop) were examined.

2. Experimental procedure

2.1. Geometric parameters of cyclone separator and dust outlet geometry

The geometric parameters of the studied cyclone separator are given in Fig. 1 and Table 1.

The dimensions of dust outlet geometries (conventional designs and with down-comer tubes) are shown in Table 2.

2.2. Experimental procedure

Experiments were performed with a 10 m/s inlet velocity for solid loading rates of 0.0–2.5 g/m^3. Arizona Test dust (Powder Technology, INC), having a density of 2650 kg/m^3, was used as feeding particles (PSD: 0.742–18 μm, SD: 1.762 μm).

A schematic diagram of the experimental setup is shown in Fig. 2. The air flow was generated using a vacuum at the end of cyclone separator outlet. Particle laden air was introduced through an extended inlet (800 mm of length) to ensure fully developed flow at the real entrance to the cyclone separator. Each experiment was conducted for 3–15 min depending on the solid concentration. To appraise the performance of cyclones concerning the geometries of the dust collection section, three parameters were considered: 1) overall collection efficiency, 2) grade efficiency and 3) pressure drop.

2.2.1. Calculating overall collection efficiency

To calculate overall collection efficiencies, the separated particles were collected by hammering and the weights were measured. Then the overall collection efficiency (η_{tot}) was calculated by Eq. (1.0) considering the ratio of the mass of particles collected (M_c) to the mass flow rate of incoming particles (M_{in}).

$$\eta_{tot} = \frac{M_c}{M_{in}} \tag{1.0}$$

Calculating overall collection efficiencies, only particles deposited on the cyclone walls and the inside dust collection hopper were taken into account, whereas particles collected inside the extended tube were ignored. This selection is appropriate for the particle loading rates considered, as the mass of deposited particles inside the tube at low particle loading conditions is lower than the mass at higher loading conditions.

2.2.2. Calculating grade collection efficiency

Two isokinematic flow volumes were extracted from the inlet and outlet by using sampling probes (VRL 50–080108, Nihon Pisco) and were diluted by supplying additional air through air blowers (see Fig. 2.0). Particle number concentrations at the inlet and outlet were measured by a Fluke particle counter (Fluke 983, FLUKE Inc.) and were considered to obtain grade efficiency curves.

Pertinent to measuring particle number concentrations by Fluke 983, the span of the particle channels are quite large; therefore, the relevant particle size fractions were considered in grade efficiency calculations rather than assuming specific particle diameters.

2.2.3. Measuring pressure drop of cyclone separator

The pressure drop in a cyclone separator is taken as the static pressure difference between the inlet and the outlet. In the present study, rather than using the static pressure, the mean pressure was measured by using an Air Flow Meter (TSI PVM 620). At the inlet, the mean pressure is uniformly distributed across a cross-section and the measurement is trouble-free. However, due to turning and sudden contraction of the flow at the outlet, the pressure averaging of the outlet is incorrect. Therefore, a realistic method conducted by Hoffmand et al. [20] was used to measure the downstream mean pressure.

3. Theoretical prediction of cyclone separators

Theoretical predictions of cyclone performance were compared with experimental results. Although there are many theories in the literature to predict cyclone performance (e.g., [21,22]), only a few are related to cyclone performance and solid loading rate (Table 3 and Table 4).

An empirical model to calculate the collection efficiency (Table 3) proposed by Smolik (quoted by Svarovsky [23]) is based on experimental results. The mechanistic model proposed by Muschelknautz et al. [24,25] is based on the phenomena of "critical load", which expresses the amount of solids that can be carried in a turbulent suspension. This theory may be the most practical method for modelling cyclone separators at the present time [26]. It is also an improvement of Barth's theory [21], which accounts the effects of particle load, wall roughness, secondary flow and changes in particle size distribution within the body on collection efficiency and pressure loss.

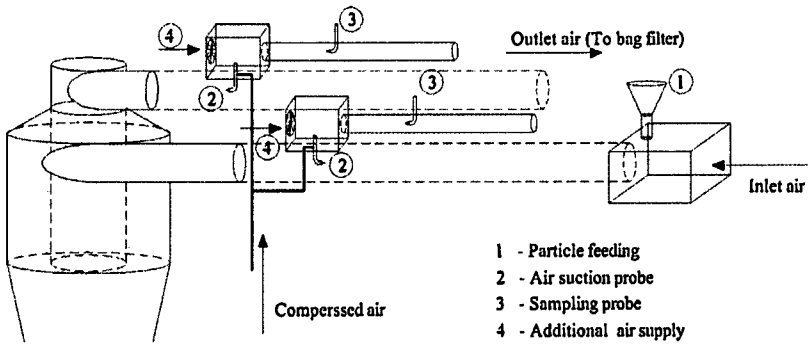

Fig. 2. Schematic diagram of experimental setup.

Table 3
Theoretical formulas of different models in the literature related to solid loading rate.

Model	Equation(s)	
Smolik	$\eta(C_2) = 1 - [1 - \eta(C_1)]\left[\frac{C_1}{C_2}\right]^{1.8}$	2.0
Muschelknautz	$\eta = \sum_{i=1}^{N} \eta_i \times \Delta MF_i$	3.0
	$C_{0L} = \frac{f' D_m \mu}{2\left(1-\frac{D_g}{D}\right)\rho_P d_{med}^2 v_{0m}}$	3.1
	$D_m = \sqrt{DD_e}, f' = 0.005\left(1+3\sqrt{C_0}\right), v_{0m} = \sqrt{v_{0w} v_{0x}}$	3.2
	$\eta_i = \frac{1}{1+\left(\frac{d_{50}}{d_x}\right)^{\overline{m}}}$	3.3
	$d_{50} = d_{fact}\sqrt{\frac{18\mu(0.9Q)}{2\pi(\rho_p-\rho_g)v_{0CS}(H-S)}}$	3.4

Table 4
Theoretical formulas of different models in the literature related to pressure drop based on the mass loading effect.

Model	Equation(s)	
Smolik	$\frac{\Delta P(C)}{\Delta P_0} = \left(1 - 0.02C^{0.6}\right)$ (units of solid loading in is in g/m^3)	4.0
Briggs	$\frac{\Delta P(C)}{\Delta P_0} = \frac{1}{\left(1+0.0086C^{0.5}\right)}$ (units of solid loading in is in g/m^3)	5.0
Baskakov	$\frac{\Delta P(C)}{\Delta P_0} = \frac{1}{\left(1+0.0086C^{0.5}\right)}$ (units of solid loading in is in kg solid/kg air)	6.0
Muschelknautz	$\Delta P_{Body} = \frac{f A_R \rho_g \left(v_{0w} v_{0CS}\right)^{1.5}}{1.8Q}$	7.0
	$\Delta P_x = 0.5\rho_g v_x^2\left[\left(\frac{v_{0CS}}{v_x}\right)^2 + K\left(\frac{v_{0CS}}{v_x}\right)^{\frac{4}{3}}\right]$	7.1
	$\Delta P_{acc} = (1+C_0)\frac{\rho_g\left(v_2^2 - v_1^2\right)}{2}$	7.2
	$\Delta P_{tot} = \Delta P_{body} + \Delta P_x + \Delta P_{acc}$	7.3
	$f = f_g + 0.25\left(\frac{R}{R_x}\right)^{-0.625}\sqrt{\frac{\eta Fr_x \rho_g}{\rho_{str}}}$	7.4
	$K = \begin{cases} 3.41 for vortex finders with rounded edges \\ 4.40 for vortex finders with sharp edges \end{cases}$ (For more details refer Muschelknautz [25,27]).	

Existing theories for pressure drop calculation (Table 4) are the empirical theories proposed by Smolik (reported by Svarovsky [23]), Briggs [28] (reported by Hoffmann and Stein [26]) and Baskakov et al. [29], while the mechanistic relationship is proposed by Muschelknautz [25,27]. The Muschelknautz method is mainly contributed from wall frictional losses, losses in the vortex core and vortex finder and those losses contributed by particle loading and flow acceleration pressure loss.

4. Results and discussion

Both visual observations and experimental results were considered to analyse the performance of the cyclone separator. For visual explanations, particle transport and deposition patterns were observed for all hopper geometries and from experimental results; collection efficiency and pressure drop were also considered.

4.1. Dust deposition inside cyclone separator

Fig. 3 shows a droplet formation of particle deposition that confirms particle agglomeration during the separation process. The particle deposition pattern on the walls differed from the continuous spiral formation observed in the literature [30,31].

Deposition on the hopper walls was also different from the conventional for hoppers combined with down-comer tubes. Com-

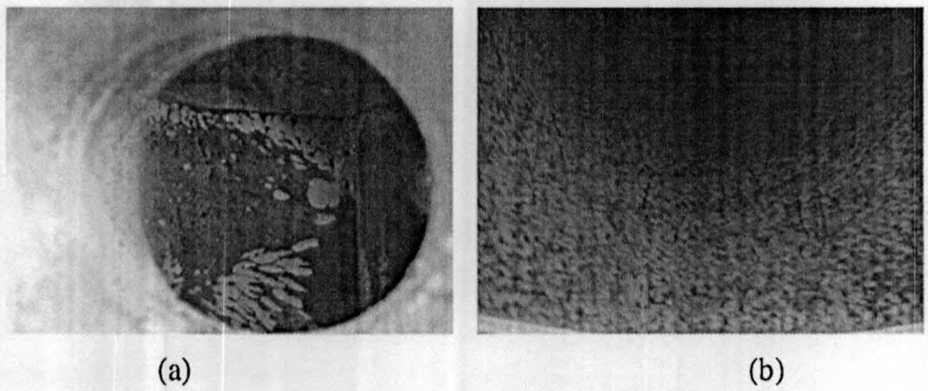

Fig. 3. Particle deposition inside cyclone walls (a) Inlet (b) Cyclone body.

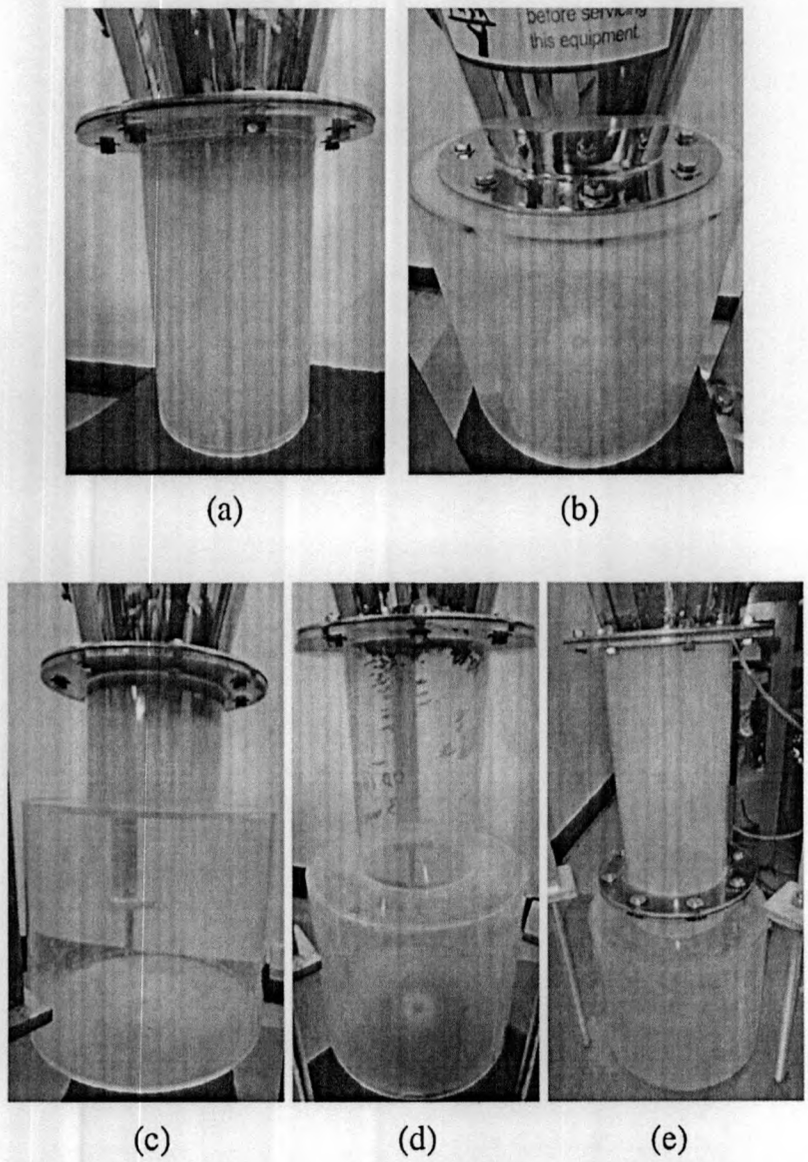

Fig. 4. Particle deposition in hoppers (a) Hopper 1; (b) Hopper 2; (c) Hopper 3; (d) Hopper 4 and (e) Hopper 5.

paring two conventional hoppers (Fig. 4(a) and (b)), the particle deposition on the walls of Hopper 1 was similar to deposition pattern on the cyclone walls, but deposition on Hopper 2 had only an insignificant layer. Considering the hoppers with down-comers (Fig. 4(c)–(e)), a droplet formation had taken place on the down-comer walls similar to the cyclone walls, and thin dust layers were on hopper walls. One interesting phenomenon shown in

Fig. 4(c)–(e) is a heavier dust deposition on the upper part of down-comer walls and a continuous reduction towards the bottom.

Particle transportation and deposition inside cyclone separators was also observed. At first all particles started to deposit on walls, followed by carrier flow (at the beginning, particle deposition in hoppers were not observed). Spiral shaped particle clouds reaching the bottom could be visualized after a while, and this observation was well noticed at high solid loadings. The particle deposition pattern is shown in Fig. 5 for Hopper 1 and for down-comer tubes of Hopper 4 and Hopper 5. Inside down-comer tubes, the trajectories of these particle clouds were horizontally spiralled at the upper part and turned angularly upon reaching the bottom of the tube. Inside Hopper 1, the spiral particle clouds were angular; inside Hopper 2, such a visible flow was not observed.

Considering solid particle deposition inside the hoppers (Fig. 6), two major deposition regions were identified: 1) at the edges of the hopper and 2) the middle of the hopper. The later deposition area contributed to the particle re-entrainment. By increasing the down-comer length, particle deposition near this area was reduced; however, at higher flow rates, the two deposited zones were connected.

4.2. Overall collection efficiency

4.2.1. Experimental results

Experimental investigations for 0–2.5 g/m^3 solid loading conditions for the considered five hopper geometries are shown in Fig. 7. The general trend of the overall collection efficiency versus solid flow rate is a dramatic increase in efficiency until 0.5 g/m^3, followed by a levelling off at high solid loadings. Identical observations were also reported by Hoffmann et al. [11,13,20]. An increase in the collection efficiency with solid loading is common in the literature [32–36], while a reduction of collection efficiency at high loading conditions followed by the collection of efficiency increments was reported by a few investigators [37,38].

Referring to the theoretical explanation of Muschelknautz's critical loading concept [24,25], the particle separation inside a cyclone separator is followed by two mechanisms: 1) mass loading effect (*i.e.*, solid mass dumps on walls immediately after entering the cyclone inlet) and 2) classification (*i.e.*, solid mass separates under the centrifugal force in the vortex flow). This clarification suggests that the overall collection efficiency increases with solid concentrations caused by the increase of solid separation by the mass loading effect. However, the present study showed relatively constant overall collection efficiencies after 0.5 g/m^3 for all hopper conditions. This can be explained as the reduction of particle separation by classification due to reductions in turbulence at high solid concentrations. Additionally, at high solid loading rates, the sudden breakup of particle wall depositions followed by downward sweeping may cause particle back mixing and also the sudden reduction in the flow swirl, which may worsen the particle separation.

Similar overall collection efficiencies were observed for Hopper 1 and Hopper 2 that contradict the previous studies [33,39], which provided evidence for cyclone collection efficiency improvement in larger diameter hoppers.

The application of down-comer tubes at the cyclone bottom is effective at low solid loading conditions, and Hopper 4 shows further improvements (Fig. 7). For better interpretation, the overall collection efficiencies for each individual dust collection condition are shown in Fig. 8.

Overall collection efficiencies at 3.6 g/m^3 and 8.0 g/m^3 are not shown in Fig. 7 and Fig. 8 and are listed in Table 5. Comparing overall collection efficiencies at these loading conditions with the efficiency at 2.5 g/m^3, the collection efficiencies were hardly affected by the solid concentrations at a high solid loading rate.

4.2.2. Results comparison with theories

The calculated overall collection efficiencies by Smolik method (Eq. (2.0), Table 3) with present experiment results are shown in Fig. 8 (by straight lines). In the calculations, the values for C_1 and η_1 were used related to 0.5 g/m^3 for each hopper design, and the dependency of the prediction curve by Smolik method onC_1 is quite obvious. If a higher value forC_1 is chosen, the prediction curve moves upward and over-predicts the efficiency at low solid loading conditions. However, the change of collection efficiency at high solid concentrations was insignificant, so choosing a higher value forC_1 did not influence this range and vice versa for smaller values. This type of dependency was reported in previous studies for extremely low solid loading conditions [32] and for higher loading rates [20].

The present study assumed another equation (Eq. (8.0)) that fits well with the experimental data (Fig. 8, dash lines) when considering the turning point of curves, from the dramatic increment to the relatively constant (in this study, 0.5 g/m^3) values of C_1 and $\eta(C_1)$.

$$\eta(C_2) = 1 - [1 - \eta(C_1)]\left[\frac{C_1}{C_2}\right]^{\left[1-\left(\frac{C_1}{\eta(C_1)}\right)\right]} \tag{8.0}$$

To compare the experimental investigations with the Muschelknautz method (Eqs. (3.0)–(3.4), Table 3), mean values of each particle fraction were considered, although experimental overall efficiencies were based on particle size fractions. Experimental and Muschelknautz predictions of overall collection efficiencies are shown in Table 6. Overall collection efficiencies from this theory and the experiments are different with respect to the geometry of the dust collection section. However, comparing all geometric conditions, the solid loading condition Muschelknautz method at 0.1 g/m^3 predicted lower efficiencies than observed with a maximum difference in Hopper 5 (25%) and minimum in Hopper 4 (9%). Overall collection efficiencies were 0.2 g/m^3, so Hopper 1 and Hopper 2 had similar results with the experiments, while Hopper 3 and Hopper 5 under-predict and Hopper 4 over-predicts. For high solid loadings above 0.2 g/m^3, overall collection efficiencies of Hopper 1 always give higher theoretical collection efficiencies; others resulted in very similar values with the experiments. The over-prediction of collection efficiencies in Hopper 1 is due to the effect of smaller wall area (A_r) in the calculations compared to other geometries.

4.3. Grade efficiency of particles

4.3.1. Experimental results

Grade efficiency curves are important in cyclone performance analysis, as they are based on the number of particles and uninfluenced by mass (mass basis representation may be affected by the number of larger particles).

For selected solid loading rates, grade efficiency curves are shown in Fig. 9 for cyclone separators with different dust collection sections.

Comparing conventional hoppers (Fig. 9(a) and (b)), the grade efficiencies are slightly higher in Hopper 2 than Hopper 1 with the provided additional separation space. Fig. 6 also shows lesser particle deposition at the re-entrainment zone of Hopper 2. However, the separation of larger particle fractions is higher in Hopper 1 with the strong tangential velocities inside.

The general trend of grade efficiency curves is an upward shifting with solid loading, and the change is dramatic for the fine particles (PM2.5). Although these particles are mostly governed by Brownian motion in nature, the strong turbulence inside the cyclone separator creates highly concentrated particle zones at higher inlet particle concentrations, which leads to particle agglomeration and increases the finer separation efficiency. However, this incremental rate of separation decreases with the down-comer

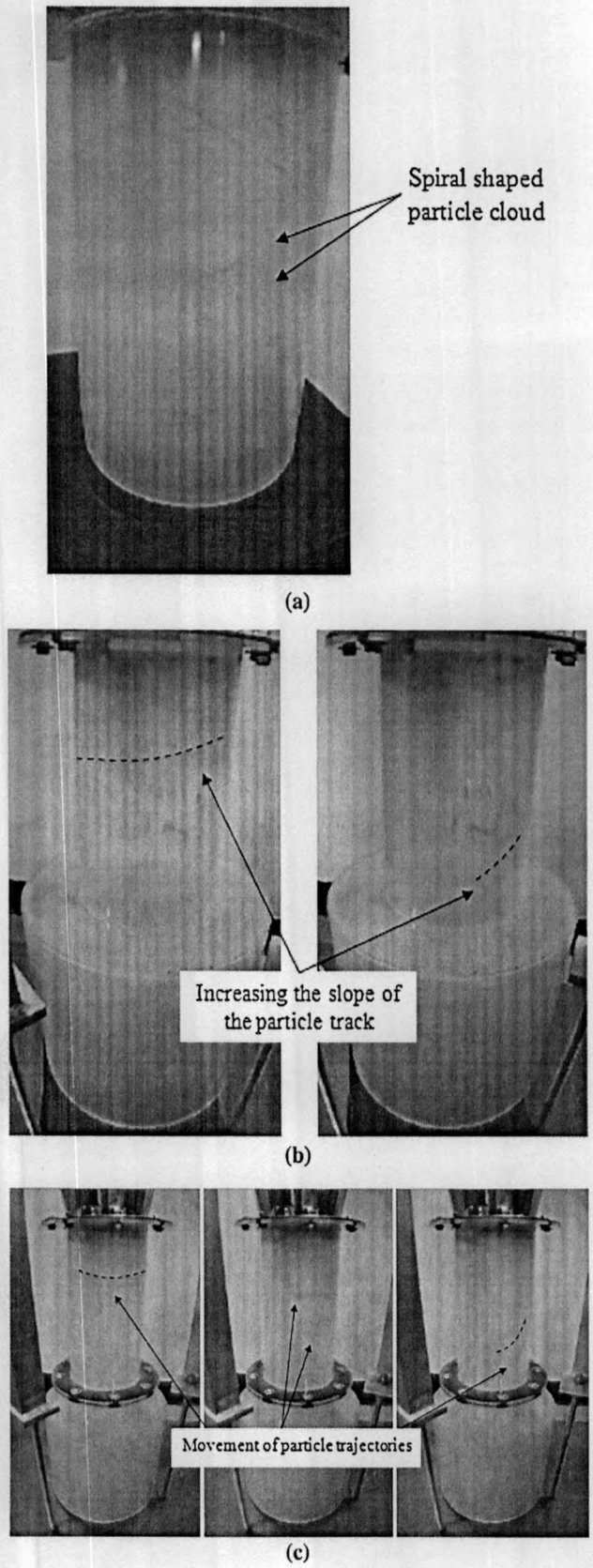

Fig. 5. Particle trajectories inside down-comer tubes (a) Hopper 1; (b) Hopper 4; and (c) Hopper 5.

length. As quoted by Ji et al. [32], turbulent particle agglomeration is significant for particle collection, especially with particles smaller than 10 μm [40]. At higher solid loading conditions, significant improvements in finer separation are also reported in the literature [12,41–45]. However, grade efficiencies of a coarser range did not correspond to the dust outlet geometry. Similar incremental

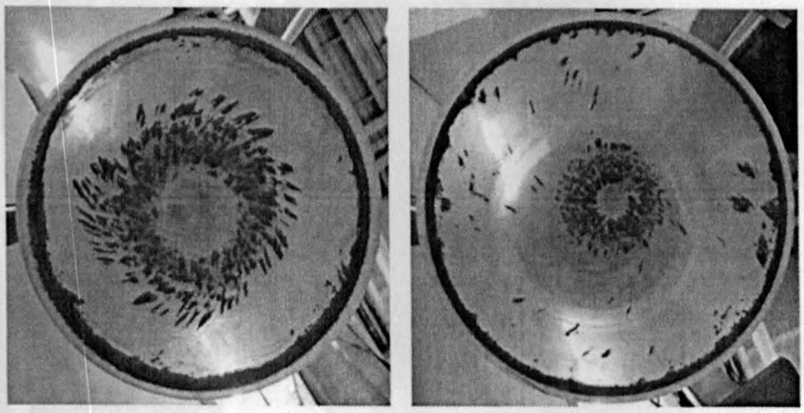

Fig. 6. Particle deposition at bottom of hoppers (a) Hopper 1 (b) Hopper 2.

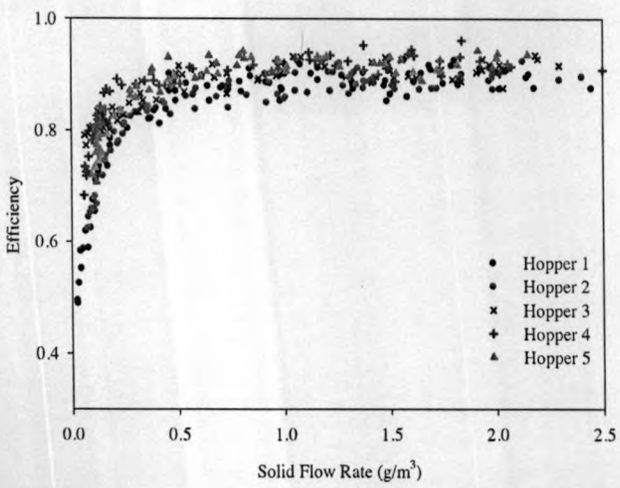

Fig. 7. Measured overall collection efficiencies for cyclone separators with different dust outlet sections at 0–2.50 g/m³ solid loading conditions.

Table 5
Overall collection efficiencies at selected solid loading conditions.

Solid loading rate (g/m³)	Overall collection efficiency				
	Hopper 1	Hopper 2	Hopper 3	Hopper 4	Hopper 5
0.10	0.658	0.673	0.803	0.792	0.736
0.20	0.787	0.778	0.832	0.881	0.818
0.50	0.871	0.851	0.906	0.883	0.895
1.00	0.885	0.871	0.929	0.926	0.920
1.50	0.879	0.888	0.909	0.892	0.918
2.00	0.890	0.895	0.906	0.912	0.927
3.60	0.903	0.855	0.888	0.902	0.894
8.00	0.886	0.900	0.888	0.899	0.895

Table 6
Experimental and calculated (Muschelknautz model) overall collection efficiencies.

Solid loading rate (g/m³)	Overall collection efficiency									
	Hopper 1		Hopper 2		Hopper 3		Hopper 4		Hopper 5	
	Exp	Musche-lknautz	Exp	Musche-lknautz	Exp	Musche-lknautz	Exp	Musche-lknautz	Exp	Musche-lknautz
0.1	0.657	0.571	0.673	0.575	0.803	0.618	0.792	0.722	0.736	0.555
0.2	0.787	0.773	0.778	0.762	0.832	0.737	0.881	0.901	0.818	0.587
0.5	0.871	0.947	0.851	0.819	0.906	0.902	0.883	0.916	0.895	0.902
1.0	0.885	0.953	0.871	0.836	0.929	0.863	0.926	0.874	0.92	0.930
1.5	0.878	0.932	0.888	0.805	0.908	0.929	0.892	0.978	0.918	0.925
2.0	0.889	0.931	0.895	0.893	0.906	0.926	0.912	0.897	0.927	0.936

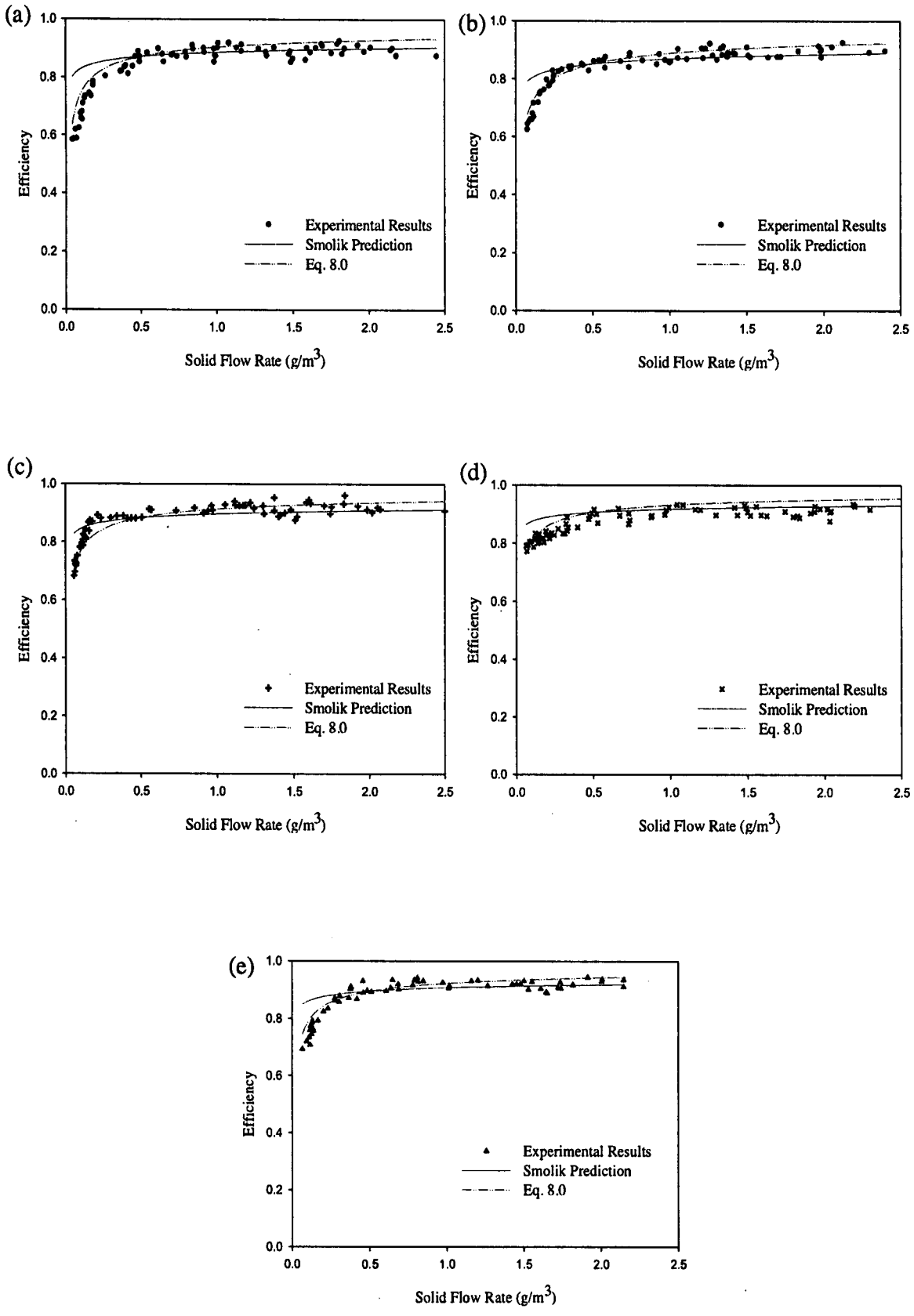

Fig. 8. Data fitted by Smolik method prediction and Eq. 8.0 with measured overall collection efficiencies for cyclones with different dust outlet conditions (a) Hopper 1; (b) Hopper 2; (c) Hopper 3; (d) Hopper 4 and (e) Hopper 5.

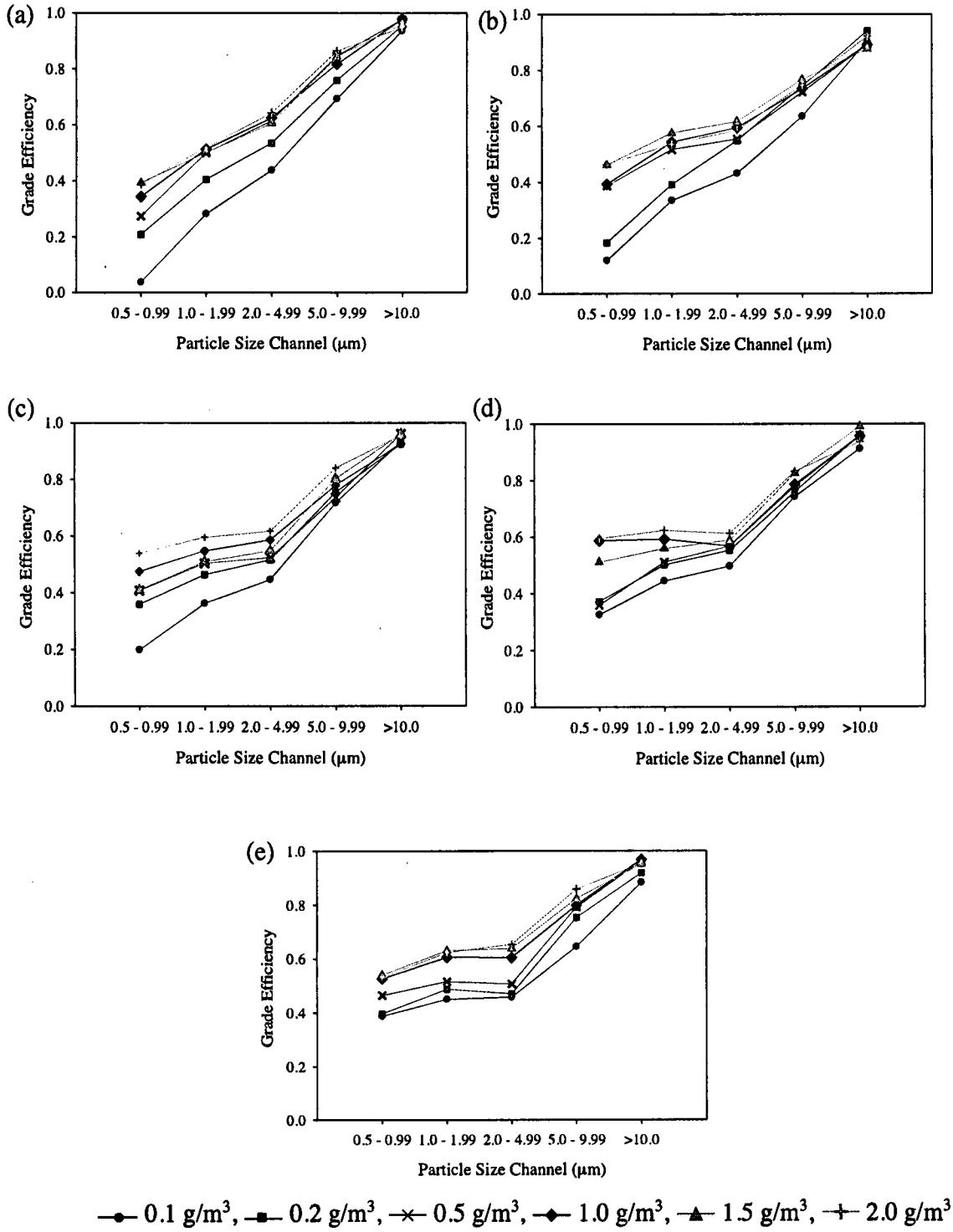

Fig. 9. Measured grade efficiency curves for cyclone separators with different dust outlet geometries (a) Hopper 1; (b) Hopper 2; (c) Hopper 3; (d) Hopper 4 and (e) Hopper 5.

behaviour in the fine particle separation was observed by Obermair and Staudinger [9] when increasing down-comer lengths from 0 to 500 mm. Kaya and Karagoz [46] reported identical results based on numerical simulations for cyclone separators with down-comers only.

"Fish-hook" shaped grade efficiency curves were obtained at 0.5–2.0 g/m^3 solid loading rates for Hopper 3 and at all solid loading conditions for Hopper 4 and Hopper 5. Similar results are found in the literature [12,42] for cyclones with down-comers and re-circulating processed flows [41,43–45]. Thus, down-comer tubes can alternate re-circulating cyclones.

4.3.2. Results comparison with theories

Experimental grade efficiency curves were compared with predicted grade efficiency curves by Muschelknautz model [24,25] (Fig. 10). Calculations used a range of 0.7–1.88 for the constant*m* (Eq. (3.3)) to obtain comparable results with experiments (differed from Muschelknautz's specifications). The geometry of the dust col-

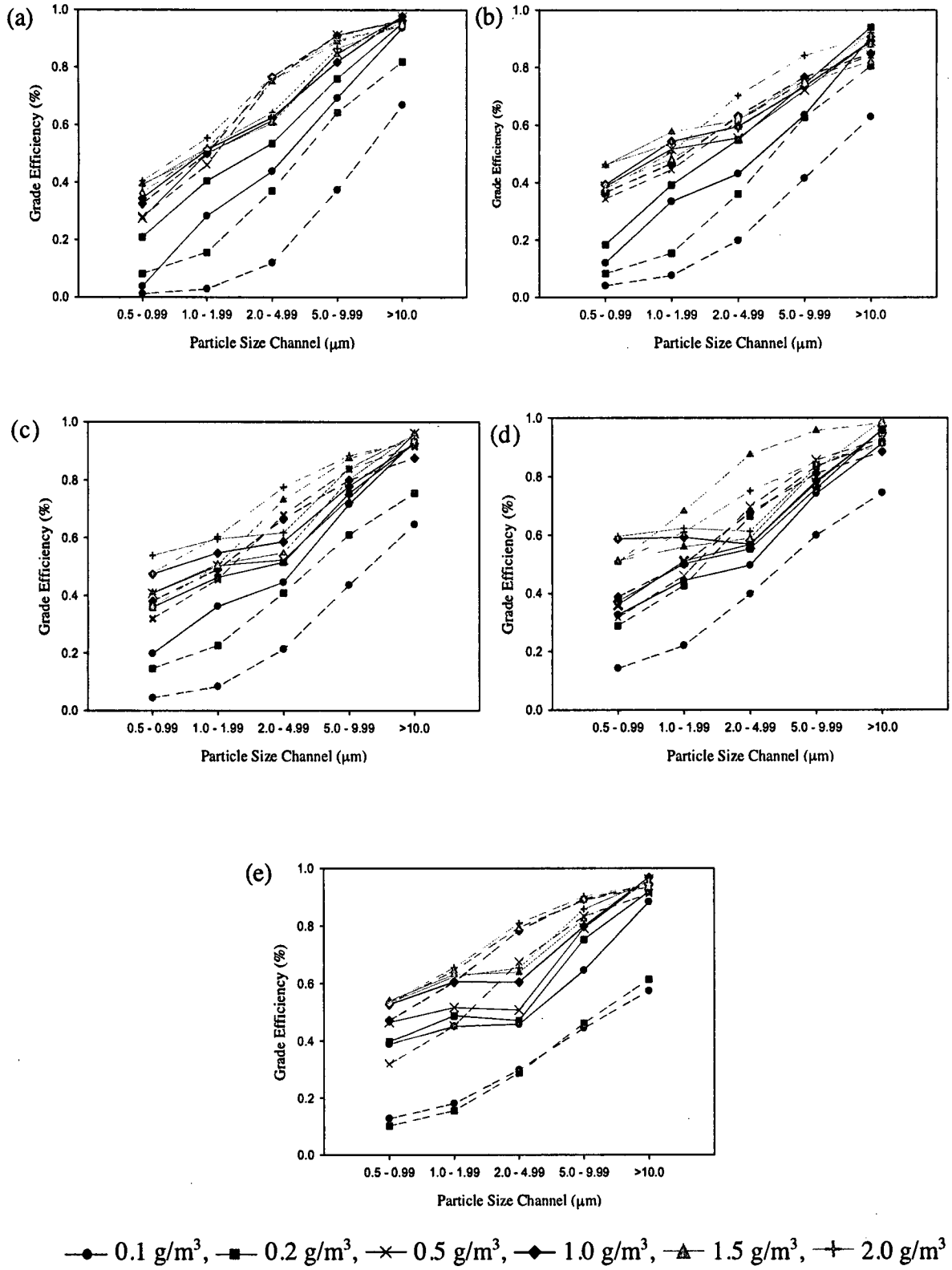

Fig. 10. Grade efficiency curves for cyclone separators with different dust outlet geometries (a) Hopper 1; (b) Hopper 2; (c) Hopper 3; (d) Hopper 4 and (e) Hopper 5 (Experimental results- Straight lines, Muschelknautz theory- Dash lines).

lection section has been included in the calculations for the total surface area (A_r) and the total height (H).

As shown in Fig. 10, the Muschelknautz method shows smooth-"S" shaped grade efficiency curves, owing to the low collection efficiencies for finer fractions and increasing collection efficiencies with particle diameter. This theory also always under-predicts grade efficiencies at low solid concentrations (<0.2 g/m^3). When the solid loading rate is higher than 0.2 g/m^3, this theory always under-predicted finer fractions while over-predicting coarser fractions (> 2 μm). However, grade efficiencies of larger particles (>10 μm)

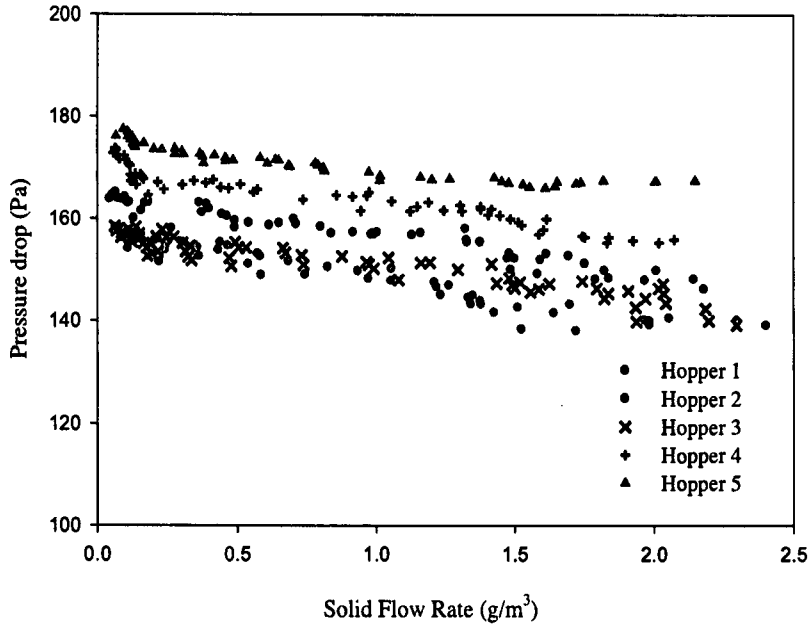

Fig. 11. Measured pressure drop values for cyclone separators with different dust outlet sections for 0.0–2.50 g/m³ solid loading conditions.

Table 7
Cut size diameters (d_{50}) from experimental and Muschelknautz model predictions.

Solid loadingrate (g/m³)	Cut size diameters (d_{50}), (μm)									
	Hopper1		Hopper2		Hopper3		Hopper4		Hopper5	
	Exp	Musche-Iknautz	Exp	Musche-Iknautz	Exp	Musche-Iknautz	Exp	Musche-Iknautz	Exp	Musche-Iknautz
0.1	5.0–9.99	9.387	5.0–9.99	9.202	5.0–9.99	4.809	2.0–4.99	4.816	5.0–9.99	9.405
0.2	2.0–4.99	4.693	2.0–4.99	4.877	2.0–4.99	1.924	1.0–1.99	1.806	5.0–9.99	8.360
0.5	1.0–1.99	1.564	1.0–1.99	1.840	1.0–1.99	1.564	1.0–1.99	1.605	1.0–1.99	1.672
1.0	1.0–1.99	1.408	1.0–1.99	1.656	1.0–1.99	1.380	1.0–1.99	1.405	0.5–0.99	0.941
1.5	1.0–1.99	1.330	1.0–1.99	1.564	1.0–1.99	0.920	0.5–0.99	0.903	0.5–0.99	0.836
2.0	1.0–1.99	1.174	1.0–1.99	1.380	0.5–0.99	0.810	0.5–0.99	0.803	0.5–0.99	0.732

Table 8
Pressure drops from experimental and Muschelknautz model predictions.

Solid loading rate (g/m³)	Pressure drop (Pa)									
	Hopper1		Hopper2		Hopper3		Hopper4		Hopper5	
	Exp	Musche-Iknautz	Exp	Musche-Iknautz	Exp	Musche-Iknautz	Exp	Musche-Iknautz	Exp	Musche-Iknautz
0.1	163.63	308.49	156.00	237.82	157.00	224.28	171.20	212.87	176.64	203.21
0.2	161.50	308.47	155.20	237.81	153.83	224.23	165.80	212.85	173.93	203.19
0.5	158.90	308.40	152.97	237.77	155.30	246.47	166.30	212.80	171.65	203.14
1.0	157.05	308.28	148.73	237.65	150.17	246.37	165.37	212.71	168.25	203.04
1.5	149.70	308.17	140.45	237.56	146.97	246.27	159.30	212.62	166.85	202.97
2.0	147.97	308.05	139.90	237.46	145.28	246.17	155.60	212.53	167.30	202.89

are close to experimental results, which can be attributed to the theoretical concern on particle sizes only and ignoring particle agglomeration.

Grade efficiency curves are important to determine the cut size diameter (d_{50}) of cyclone separators, which is the particle size corresponding to a 50% collection efficiency. All particles having larger diameters than this will be collected with a fraction above 50%. d_{50} for each cyclone separator (consistent with the particle fraction ranges in Fluke 983) at selected solid loading rates are given in Table 7 for comparison with the results calculated from the Muschelknautz theory. To obtain comparable results from the theory to match the experimental results, the modification factor (d_{fact}) for d_{50} defined in the theory was inapplicable (Eq. (3.4)) and the range of 0.24–3.2 was used.

d_{50} values of the Hopper 1 and Hopper 2 are nearly the same. Although Hopper 3 shows higher collection efficiencies at low solid concentrations (Fig. 8(c)), the d_{50} value is not smaller as expected. However, among five dust outlet geometries, Hopper 4 has smaller d_{50} values than the others, which is already considered as the geometry with the best performance in particle separation.

4.4. Pressure drop

4.4.1. Experimental results

Pressure drop distributions with a solid loading rate are shown in Fig. 11 for each cyclone separator with different hoppers. It is obvious that the increase in solid loading reduces the pressure drop in Fig. 11 for each geometric condition and increases with the down-comer height. However, comparing two conventional hop-

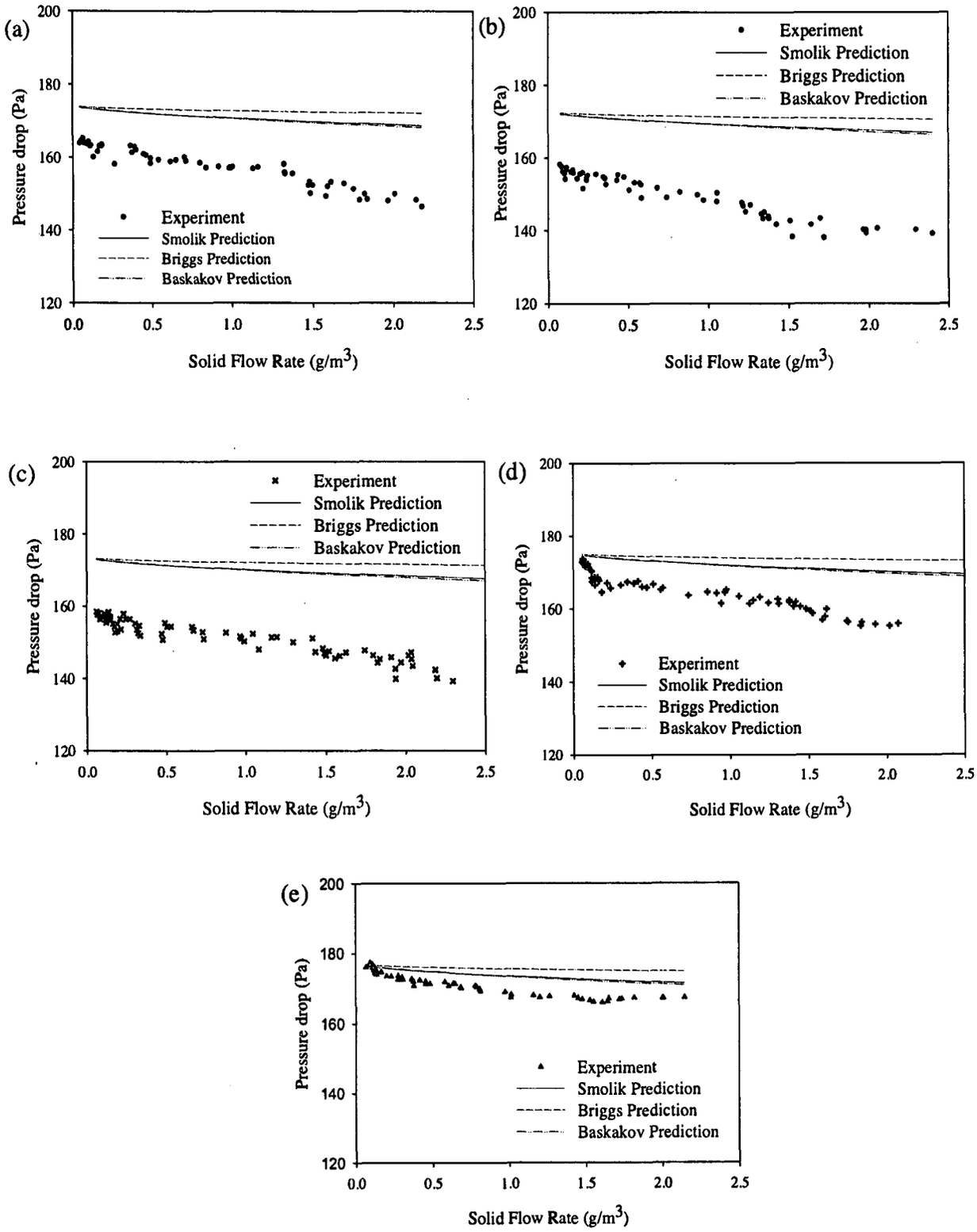

Fig. 12. Measured and theoretical pressure drops in cyclone separators with different dust outlet geometries (a) Hopper 1; (b) Hopper 2; (c) Hopper 3; (d) Hopper 4 and (e) Hopper 5.

per designs, Hopper 1 shows a higher pressure drop than Hopper 2. Although there is a sudden extraction at Hopper 2, the higher pressure drop in Hopper 1 is a dramatic dissipation of kinetic energy at high tangential velocities.

Pressure drops in Hopper 3 are smaller than Hopper 4 and Hopper 5, and almost coincides with the pressure drops of Hopper 2 up to the solid loading of 1.0 g/m^3 and higher at high solid concentrations. The reason for the former behaviour may due to a lower increment of wall area and tangential velocity in Hopper 3 in comparison with Hopper 2; also, the short down-comer tube contributes far less tangential velocity increment of flow in Hopper 3. Pressure drops are thus similar in both cyclones at solid con-